Mixture Formation in Direct Injection Hydrogen Engines: CFD and Optical Analysis of Single- and Multi-Hole Nozzles

Author, co-author (Do NOT enter this information. It will be pulled from participant tab in MyTechZone)

Affiliation (Do NOT enter this information. It will be pulled from participant tab in MyTechZone)

ABSTRACT

This paper describes the validation of a CFD code for mixture preparation in a direct injection hydrogen-fueled engine with a single-hole and a multi-hole nozzle. Numerical results from the commercial code Fluent (v6.3.35) are compared to measurements in an optically accessible engine. The cylinder geometry is typical of passenger-car sized spark-ignited engines, with a centrally located injector. Quantitative planar laser-induced fluorescence provides phase-locked images of the fuel mole-fraction, while single-cycle visualization of the jet penetration is achieved by a high-speed schlieren technique. The characteristics of the computational grids used in this work are discussed, with particular regard to the near-nozzle region where the jet is under-expanded.

Simulation of injection from the single-hole nozzle yields remarkable agreement between numerical and optical results in terms of jet penetration and overall evolution. The multi-hole (13-hole) nozzle has high jet-to-jet interaction, with several jets merging into a single jet immediately downstream of the nozzle. This phenomenon (usually referred as Coanda Effect) is more challenging to the numerical simulation and requires higher level of detail in numerical simulation and grid resolution, with particular regard to the fields near the injector nozzle.

INTRODUCTION

Hydrogen has been intensively researched as a fuel for ICEs for several decades [1,2,3] due to its potential to provide both high engine efficiency and low environmental impact, with NO_X as the only toxic pollutant. One of the main advantages of using hydrogen as fuel in spark-ignition (SI) engines is the wide flammability range, which allows high efficiency in most of the operating conditions while minimizing NO_X emissions. While a large-scale utilization of H_2 is curbed by the well-known challenges associated with production, distribution and on-board storage, hydrogen engines can nowadays show performance that cannot be achieved by conventional SI engines [4,5].

The U.S. Department of Energy started funding experimental activities on H_2-ICEs at Argonne National Laboratory in 2005 with challenging goals, including 45% brake thermal efficiency (BTE) and NO_X emissions of 0.07 g/mile, together with a power density comparable with gasoline engines at a mass-production cost of 30 $/kW [6]. Another important requirement was to avoid unsafe conditions due to irregular combustion (pre-ignition, backfire).

Direct injection is the most promising strategy to meet all the requirements mentioned above [7]. In particular, the risk of backfire can be avoided and the volumetric efficiency losses due to low H_2 density are eliminated, thus allowing the same or higher power density than from conventional gasoline engines. As far as efficiency and emissions are concerned, the engine optimization is highly dependent on the mixture formation process. DI engines require great effort in the optimization process since the number of degrees of freedom increases, compared to port fuel injection (PFI). In particular, the injection strategy including engine operating parameters (injection timing) and geometry (injector location, nozzle configuration) has a significant influence on the mixture formation process, which consequently affects combustion and pollutant formation. In addition, jet-to-jet interaction has to be taken into account for multi-hole nozzles.

In order to meet DOE's targets, Argonne National Laboratory has been carrying out intensive research on advanced direct injection and mixture formation concepts [8,9,10] in a single-cylinder engine. An intuitive way to increase engine efficiency is to reduce the

individual efficiency losses. To this aim, new injector technologies (piezo-actuated driver) allow performing late injection (thus reducing the losses for compression work) and delivering higher mass flow rates during injection, thus extending the operation range to higher engine load and speed, where the maximum efficiency can be achieved. Moreover, research on DI gaseous engines is extremely focused on optimizing the injection timing (start of injection, SOI) and nozzle geometry to pursuit the "ideal" stratification, consisting of a relatively rich mixture close to the spark-plug and low amount of fuel close to the cylinder walls, at spark timing. This best case scenario would provide high stability during combustion (low COV) due to the enhanced development of the early flame kernels, low NO_X emissions due to highly stratified mixture (rich and ultra-lean mixtures produce much lower NO_X than slightly lean mixtures), and significantly reduced loss for heat transfer to the cylinder walls, which happens to be the highest efficiency loss in almost every condition [11]. Strategies to further reduce NO_X emission like EGR and water injection have also been investigated [12,13], nevertheless DI H2-ICEs have the potential to provide NO_X emissions within the most severe regulation limits without the need for any after-treatment device.

Despite the extensive research in terms of advanced mixture formation, basic experimental activities cannot provide a comprehensive understanding of the physics underlying the in-cylinder processes which significantly affect performance and emissions in a DI engine, where the mixture is internally formed. Laser-based measurements in optically accessible engines can overcome this limitation and provide insight into the mixture formation process. To this end, Sandia National Laboratories have been carrying out optical investigations on a single-cylinder engine with similar geometry Argonne's all-metal engine. Via planar laser-induced fluorescence (PLIF) and particle image velocimetry (PIV), air/fuel mixing and its interaction with the intake-induced flow have been examined for injection from single and multi-hole nozzles [14,15,16].

Optical investigations on ICEs not only offer insight into the in-cylinder processes but also provide the proper experimental data for the validation of numerical results provided by a Computational Fluid Dynamic (CFD) approach. 3D-CFD investigations of mixture formation have been performed at Argonne National Laboratory with the aim to develop a tool able to provide important input to the experimental testing for the optimization of engine parameters and geometry. Despite the need to constantly verify the accuracy of numerical results by means of the comparison with experimental (and optical in particular) data, a reliable computational code can be used to predict engine performance and drastically reduce production cost for prototypes and testing time. Even operating conditions which may not be easily explored can be simulated and moreover the access to numerical results allows obtaining a wide range of information on the spatial distribution of the most relevant physical and chemical quantities within the cylinder. Accordingly, effort has to be put into ensuring reliability and accuracy of computational codes, which can be assessed by means of validation against experimental data.

This paper expands previous validation work [17,18] by widening the range of analyzed cases, including different injection pressures and different nozzle geometries. Single- and multi-hole nozzles, at high and low injection pressure, are evaluated. Simulations performed in this paper use the commercial code Fluent (v6.3.35) and a Reynolds-Averaged Navier Stokes (RANS) approach to model in-cylinder turbulence. Phase-locked PLIF measurements provide a quantitative comparison for numerical results during mixture formation. In addition, high-speed schlieren images are used to reduce numerical uncertainties related to the injection timing and early-injection transients. Numerical assumptions related to the injection profile are discussed in detail. Grid requirements are also highlighted, with particular regard to the near nozzle domain where the gaseous jet is highly under-expanded due to the high injection pressures. Once validated, the numerical approach will be able to guide the optimization of DI engines fuelled by gaseous fuels like hydrogen, but also natural gas or gaseous blends.

EXPERIMENT

OPTICAL ENGINE

The optical engine is a passenger-car sized, four-stroke single-cylinder research engine, adapted to operate with hydrogen. Large transparent segments make the engine optically accessible for laser-based measurements. Schematics of the relevant optical and mechanical components are shown in Figure 1a. The engine has a four-valve head with a pent-roof combustion chamber. The piston is flat-topped. The intake system consists of two intake ports, one for each valve, both straight and parallel to each other forming an angle of 40° with respect to the fire deck (horizontal). For this study, a full-length fused-silica liner is used, so that the entire volume swept by the piston is optically accessible, but not the pent-roof.

The main engine geometrical and operating parameters are given in Table 1. The crank-angle convention used in this paper assigns 0°CA to compression TDC. Thus, crank-angles during the compression stroke are negative. Hydrogen is supplied directly into the combustion chamber via a solenoid injector from Westport Inc. Figure 1b shows the injector location, central between the four valves. Two nozzles are used in this work, the first being a single-hole (1-h) nozzle with a hole diameter of 1.46 mm, aiming at the intake squish region (between the two intake valves) and downward, with a 50° angle with respect the injector axis. The jet axis is aligned

with the mirror-symmetry plane of the combustion chamber. The second nozzle (13-h) has 12 holes with a diameter of 0.36 mm at a 30° angle with respect the injector axis and a central hole with a diameter of 0.38 mm.

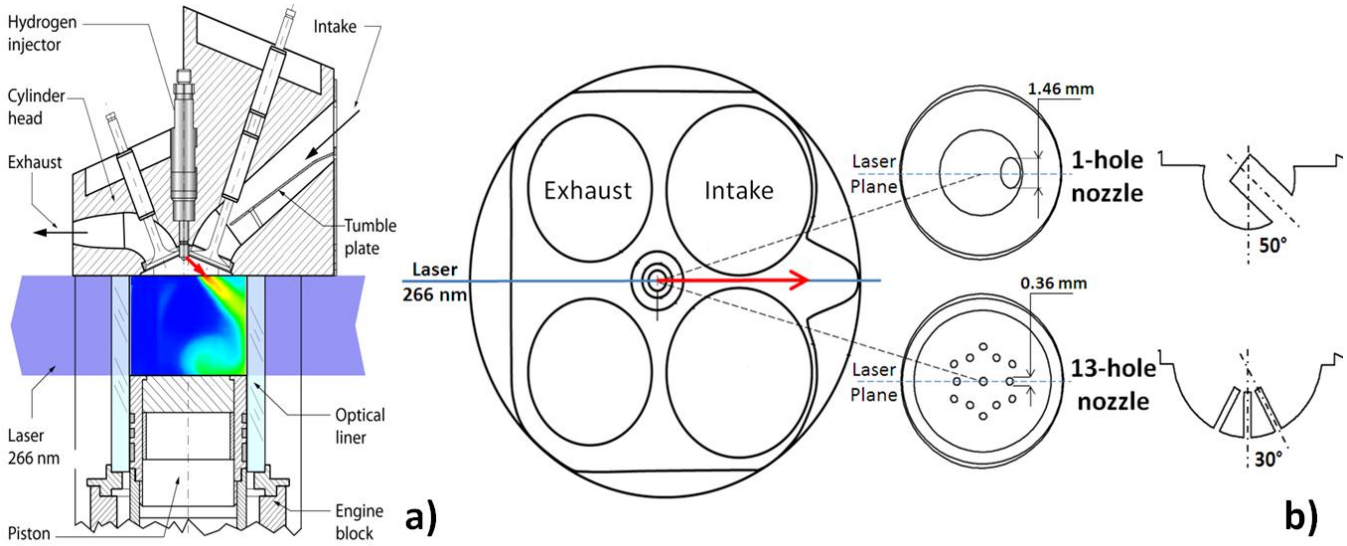

Figure 1 Schematics of engine hardware. (a) Optical engine with measurement plane. (b) Location and targeting of the nozzles with respect to the combustion chamber.

Since the present study focuses on mixture-formation prior to ignition, fired engine operation is not necessary. The engine is motored at a constant speed of 1500 RPM, and nitrogen is supplied as a bulk gas (but treated as air in calculations of the equivalence ratio). The pressure in the surge tank upstream of the intake runner is kept at 1 bar and typical intake temperatures just upstream of the engine head are around 36°C.

In all the examined operating conditions, hydrogen injection is adjusted to obtain a global equivalence ratio of 0.25 ($\lambda = 4.0$), or a hydrogen mole-fraction of 0.095. In fired operation, at typical efficiencies, this fuel concentration represents a low-load condition with about 2.5 bar IMEP. The mean fuel flow is measured far upstream of the injector with a thermal mass-flow meter (Brooks SLA5860).

Table 1 Optical engine specifications and main operating parameters

Bore / Stroke / Displacement	92 mm / 85 mm / 565 cm^3
Compression ratio	11
Speed	1500 rpm
Intake pressure / Temperature	1 bar / 36°C
Intake Valve Closing (IVC)	-140°CA
Nominal - Actual SOI delay	3°CA (at 1500 RPM)
H_2 Injection Pressure	25 and 100 bar

PLIF MEASUREMENTS

Planar laser-induced fluorescence (PLIF) of gaseous acetone as a fuel tracer is adapted to obtain quantitative images of the hydrogen mole-fraction in the operating engine. The imaging technique is described in detail in previous work [19] and is therefore discussed only briefly here. Gaseous acetone is seeded as a tracer into the hydrogen fuel by a high-pressure bubbler. At 100 bar pressure and room temperature, a volume concentration of 0.33% can be reached. For current purposes, differential diffusion of tracer and fuel is estimated to be insignificant due to the large spatial structures examined here and the high Reynolds number of the post-injection flow. Phase-locked to a particular crank angle, a quadrupled Nd:YAG at 266 nm laser excites acetone fluorescence, which is imaged onto a back-illuminated CCD camera.

Standard background and flat-field corrections are performed to quantify the measurements. For the latter, a nearly homogeneous charge is prepared by DI during the intake stroke. Distortion due to the curved liner is corrected. Inhomogeneities in the temperature field, induced by mixing of cold hydrogen and hot bulk gas, are accounted for based on known spectroscopic properties of the tracer [20,21] and on the assumption of adiabatic mixing between fuel and bulk gas [22,23,24]. The overall typical maximum error in the ensemble-mean equivalence-ratio fields is estimated to be 25%. Small regions in the images, in particular for early crank angles, may have larger errors because of local window fouling and signal reflections. 90 images of the hydrogen mole-fraction are collected at each crank-angle. The resulting sequence of phase-locked mean images has already been reported in a previous publication [16] for the case of the single-hole nozzle.

HIGH-SPEED SCHLIEREN DATA

Hydrogen-jet penetration is visualized by schlieren imaging with a high-speed camera, illustrated schematically in Figure 2. Since schlieren techniques have been used for many years to visualize density gradients in transparent media [25], only a brief description of the optical system will be given in this paper. The arrangement is that of "focused shadowgraphy" in "Z" layout [25] with the engine's cylinder and pent-roof as the imaged object. Light from a green, pulsed, high-power light-emitting diode (LED) was focused through an aperture with 0.7 mm diameter and collimated by a parabolic mirror with a focal length of 900 mm. After and before passing through the engine, cylindrical correction lenses keep the light collimated. The beam is then focused by another, identical parabolic mirror through a round aperture with 1.7 mm diameter, which acts as a schlieren stop. A camera lens with focal length f = 100 mm projects the resulting schlieren images onto the detector of a high-speed complementary metal-oxide-semiconductor (CMOS) camera (Phantom v7.1). Single-cycle sequences of images are acquired with a temporal frame spacing of 0.5°CA (= 55 μs) and an effective exposure time of 5.5 μs, given by the LED's pulse width. The visual contrast in the schlieren images is enhanced by temporal differentiation, i.e., by subtracting the previous frame from each frame [26].

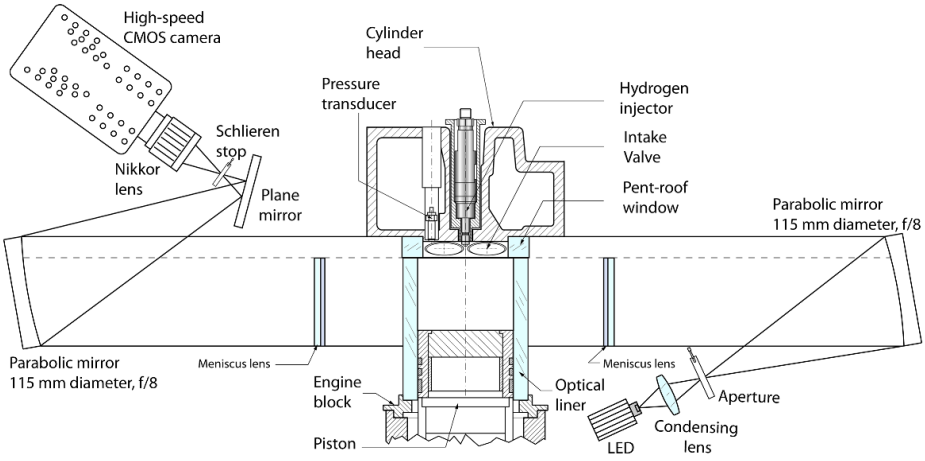

Figure 2 Schematics of the high-speed schlieren imaging technique

NUMERICAL SIMULATION

CFD simulations of direct injection of hydrogen and mixture formation are performed using the commercial CFD solver Fluent (version 6.3.35). This study follows a RANS approach combined with a k-ε model to describe in-cylinder turbulence. The quality of the RANS results is not comparable to more detailed approach such as LES or DNS, which nevertheless are not computationally affordable yet for engine applications, characterized by large computational domains and high Reynolds numbers. These two main issues significantly increase the grid resolution and consequently the computational time. However, the possibility to switch to more detailed analysis in the future will be assessed later in the paper. All the formulations of the k-ε model provided by Fluent (k-ε standard, k-ε RNG, k-ε realizable) have been previously tested and showed only slight differences in the numerical results [18]. In this paper, the Realizable k-ε is used.

The Gambit software is used as pre-processor to generate the computational grids. The numerical approach followed in this study has been comprehensively documented before [17] and therefore is only briefly summarized here:

- A computational grid for the full engine geometry (including valves and ducts) is used to compute the in-cylinder flow-field during the gas-exchange phase, prior to fuel injection.

- A computational grid of the geometry reduced to the combustion chamber only (including the nozzle geometry) is used to simulate direct injection and mixture formation.
- The flow field, state variables, and turbulence-model parameters calculated from the gas-exchange phase (step 1) are set as initial conditions for the subsequent simulation of direct injection and mixture formation (step 2).

By this approach, for a specific operating condition (engine speed and load), different injector geometries (number of nozzles, nozzle diameter, direction and location) and injection strategies (injection pressure and timing) can be evaluated on the reduced grid without the need to re-calculate the pre-injection flow-field. Furthermore, the high-pressure DI process with its transient supersonic jet requires higher grid resolution than the simulation of the gas exchange. Accordingly, the two processes are separated and two different grids are used.

This study focuses on hydrogen direct injection and mixture formation, therefore only the part of the cycle calculated with the reduced geometry is considered. However, the in-cylinder conditions (velocity field, physical quantities, chemical species) prior to SOI were previously calculated [17] and are taken into account in the present analysis. The only additionally required information is the boundary condition related to the fuel injection. To this aim, the hydrogen mass flux through the nozzle is calculated from the measured mean mass-flow rate, injection duration, and nozzle diameter, and is set as the mass-flow-inlet boundary condition for the injecting surface. The mass-flow-inlet condition is chosen, due to the lack of information about the instantaneous pressure at the injecting surface. Fuel properties at the critical section might be roughly evaluated by the assumption of sonic flow conditions but the actual pressure and temperature values at the injecting surface are difficult to calculate without explicitly modeling the flow within the injector. Also, the mass-flow-inlet condition has proven to provide more stable numerical solution than the inlet pressure condition. The only remaining issue in this analysis is how to model the jet transient, provided that during the central part of injection a quasi-steady flow can be assumed.

The instantaneous mass flow is not experimentally measured. Information on injection current, voltage and needle lift were provided by the injector manufacturer and were utilized to assume a constant injection profile, with linear ramp-up and ramp-down as shown in Figure 3. Here, the injection profile for a single-hole jet injected at 100 bar is reported, with SOI = -140°CA. The choice of the proper ramp slope and, consequently, of the transient duration for each test case examined in this work is discussed in more detail later in this paper. The resulting total mass injected per cycle (proportional to the area under the trace in Figure 3), corresponds to that calculated from the experimental multi-cycle mean hydrogen flow rate (3.46 g/cycle for all the examined cases). At the end of injection (EOI), the boundary condition for the injecting surfaces is changed from mass-flow-inlet to wall.

Experimentally, at 1500 RPM a delay of about 3°CA is observed between the injector opening command and the actual start of injection (SOI). Accordingly, for a nominal value of SOI = -140°CA, the mass flux through the nozzle begins at -137°CA. During the compression stroke a 0.5°CA time-step is used for simulation, with the exception of the injection duration, where the supersonic flow requires a smaller (0.1°CA) time-step for stable calculations.

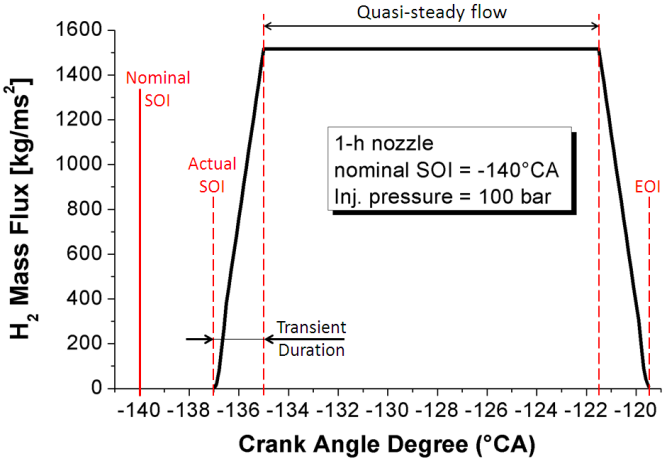

Figure 3 Schematic of the assumed generic injection profile

A detail of the grid resolution in the near nozzle domain is shown in Figure 4. Both (for the single-hole and 13-hole nozzle) the computational grids are optimized to reduce the overall number of cells and maintain the accuracy of numerical results. Accordingly, the overall cell size is slightly increased with regard to previous studies [17,18], while the mesh is locally refined in the proximity of

the nozzle. Overall grid resolution (including the boundary layer at the cylinder walls) has a significant influence on numerical results in a direct injection process, however the main influence stems from the cell size within the nozzle and at the nozzle exit [18,27], where the jet is under-expanded and great care of the grid size has to be taken, in order to predict the evolution of the supersonic jet and, consequently, jet penetration. The refinement along the jet direction allows providing a more detailed analysis of the under-expanded region, and is carried out in this paper in order to highlight the characteristics of supersonic jets. The different size (Figure 4) of the domain where the grid resolution is increased can be justified with the different value for the hole diameter (1.46 mm against 0.36 mm), which leads to a different size of the under-expanded region. Whole mesh size is 850,000 cells for the 1-h nozzle and 1,200,000 for the 13-h nozzle, both measured at IVC.

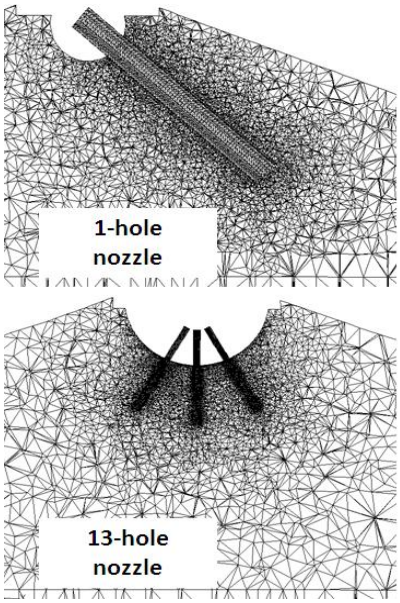

Figure 4 Local refinement in the near-nozzle region for the computational grids used in this study

RESULTS AND DISCUSSION

TEST CASES

Starting from the conditions within the cylinder at IVC (-140°CA), the present analysis focuses on the mixture formation process. As mentioned above, the main engine parameters (engine speed and load, intake pressure) are kept constant for all the examined operating conditions. Accordingly, conditions within the cylinder prior to SOI are identical. Three cases are analyzed in this paper, as listed in Table 2. This set of cases provides a proper mix of data to evaluate the mixture formation process, since significant variations in terms of injection pressure, injection duration and nozzle geometry are taken into account. The choice of early injection (SOI = -140°CA and -137°CA) can be emphasized by noting that the most severe conditions to be simulated are those where a significant amount of time is available for the fuel jet to evolve and for mixture formation to occur. Accordingly, the accuracy of the numerical results will be assessed not only in terms of fuel penetration but also in terms of mixture stratification at the end of the compression stroke.

Table 2 Examined test cases

	Test Case 1	**Test Case 2**	**Test Case 3**
Nozzle	1-h	1-h	13-h
Injection Pressure	100 bar	25 bar	86 bar
Nominal SOI	-140°CA	-137°CA	-140ºCA
Actual SOI	-137°CA	-134°CA	-137°CA
Injection duration	17.5°CA	74.5°CA	21°CA

INJECTION PROFILE

In previous studies [17,18], a trapezoidal injection profile, with injection at constant mass flux and 1°CA ramp-up and –down, was used. This assumption was accurate enough to yield good agreement between numerical and experimental (PLIF) results along the entire compression. High-speed schlieren data allows evaluating whether the transient modeling is accurate. In Figure 5, two different injection profiles (with 1°CA ramp and 4°CA ramp) are used to simulate the same operating condition (test case 1) and the numerical results in terms of H_2 mole-fraction are compared with schlieren data. The side grid-lines identify the boundaries for the schlieren imaging, therefore a comparison during the transient between CFD and schlieren data is useful only up to -134°CA (the jet reaches the right boundary). Figure 5 shows that the transient influences the jet penetration, in that the slower starting transient yields slower penetration, and that the agreement between modeling and experiments improves with a higher transient duration. Furthermore, the assumption of transient duration does not significantly affect overall mixture formation, because the differences become negligible at the end of injection (-120°CA) and at the end of compression stroke (-30°CA) where, despite the drastic reduction of the displayed H_2 mole-fraction range, the difference in terms of fuel concentration between the two numerical results is very small.

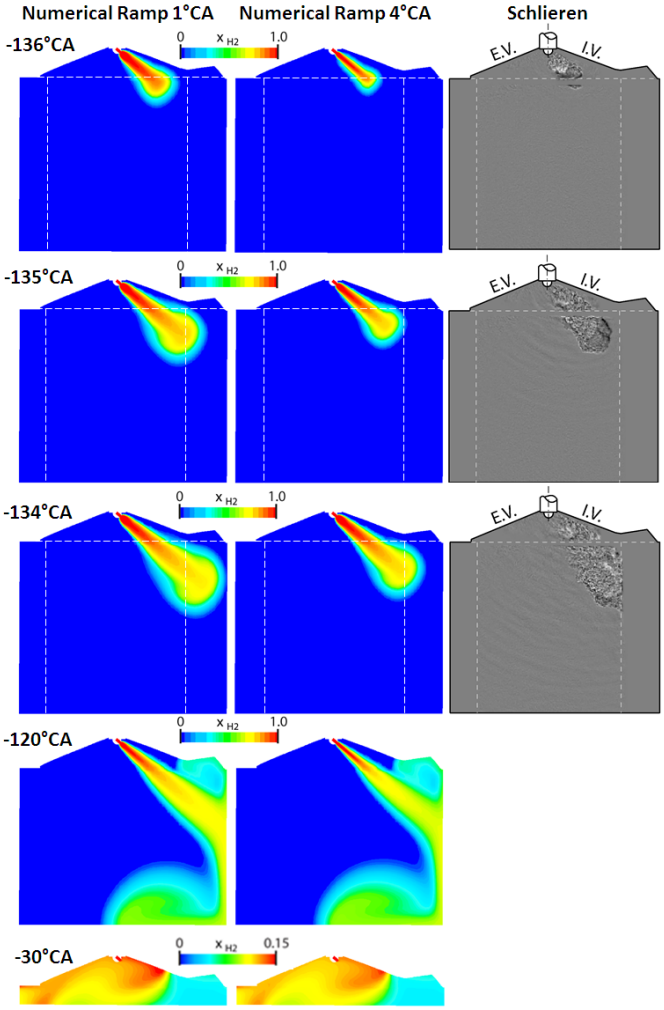

Figure 5 Influence of transient modeling on jet penetration and overall evolution (test case 1)

The comparison with high-speed schlieren data suggests that a transient duration (ramp) of 4°CA is more accurate in describing the rise of the mass-flow rate through the nozzle in test case 1 (100 bar injection pressure). The same ramp is used to model the transient for test case 2 since the injection pressure is similar (86 bar). For the low-pressure case (test case 3, 25 bar injection pressure), a ramp of 1°CA is chosen, due to the much lower values of maximum mass flux (see Figure 6), in order to assume the same mass flow rise of the high-pressure cases during the transient. The mass-flow is related to the pressure value upstream of the nozzle, therefore the present approach basically consists of assuming linear pressure rise up to the quasi-steady flow condition. As mentioned earlier, the choice of a mass-flow-inlet boundary condition for the direct injection process is due to more stable numerical solution as well as to

uncertainties about the pressure values at the injecting surface. Nevertheless the code calculates the pressure values at the boundaries on the basis of the mass flux provided and temperature condition (300 K) imposed at the inlet surface.

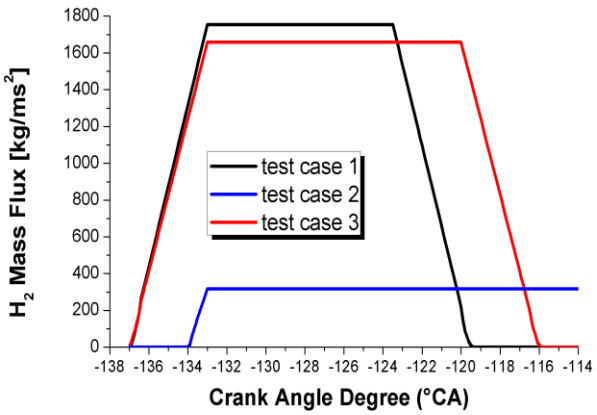

Figure 6 Injection profiles assumed in the examined test cases

SUPERSONIC JET CHARACTERISTICS

The characteristics of the under-expanded jet are calculated based on the mass-flow (imposed), pressure (calculated) and temperature (imposed) upstream of the critical section. If the ratio between injection pressure and ambient pressure is higher than the critical ratio (1.889 for H_2), the flow will take place under sonic conditions, with the mass flow rate through the nozzle being choked and depending only on the conditions upstream of the nozzle and not on the ambient properties. Figure 7 shows the maps of Mach number and absolute pressure in the near-nozzle domain for the three test cases presented here.

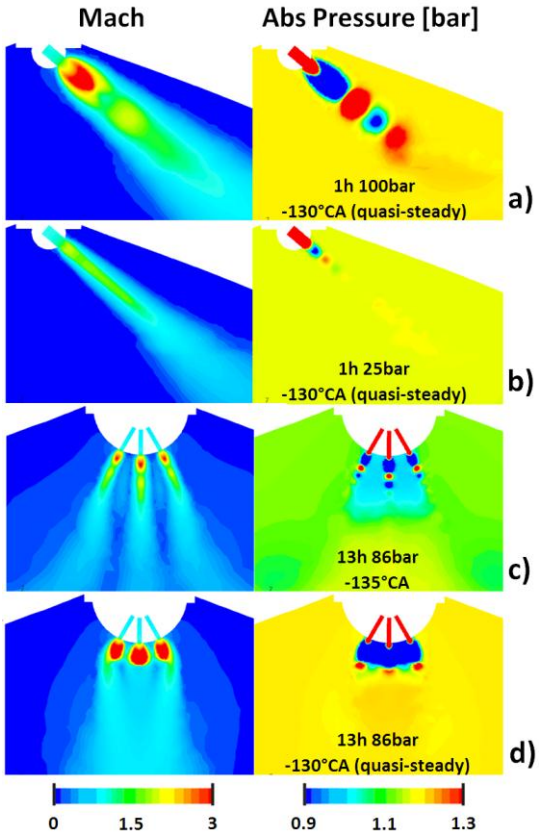

Figure 7 The under-expanded region for the examined test cases. (a) Test case 1 at quasi-steady conditions. (b) Test case 2 at quasi-steady conditions. (c) Test case 3 during transient, 2°CA after SOI. (d) Test case 3 at quasi-steady conditions

In all the examined cases a supersonic region (Ma > 1) can be seen at the nozzle exit, where the pressure switches from the injector conditions to the ambient conditions through a series of shocks along the jet direction. When the jet is highly under-expanded (high injection pressure) the recompression takes place normally through a large disk (usually referred as Mach disk) where the flow switches from highly supersonic (Ma >> 1) to subsonic (Ma < 1), which be seen in Figure 7a. The low injection pressure case (25 bar, Figure 7b) does not show a highly under-expanded jet and a clearly-visible Mach disk, even though small shocks are present and the flow is still supersonic at the nozzle exit. For test case 3 (13-h nozzle), Figure 7c shows the initial formation of separate supersonic flows downstream of each hole, where each jet is highly under-expanded with smaller Mach disks than the ones observed for the single-nozzle hole. This is in agreement with results reported in the literature that show that the Mach disk size is related to the hole diameter. After the Mach barrel region, the jets interact with each other and subsequently merge into a single jet, due to well-known Coanda effect, which leads to the formation of a single, bigger under-expanded region (Figure 7d).

A higher resolution of the under-expanded jet is prohibited by the required drastic increase in the local grid resolution, which at the same time affects the overall mesh size. In a typical under-expanded jet, the supersonic region is characterized by normal shocks and oblique reflected shocks along the jet direction, where in some cases more than one highly supersonic region (where Ma >> 1) is visible. While this phenomenon affects the air entrainment (occurring only in the subsonic region), a previous study [18] has shown that even with a lower resolution mesh of the supersonic region, it is possible to achieve a good agreement with optical data in terms of mixture formation.

TEST CASE 1 (1-H 100 BAR)

Figure 8 shows the comparison between numerical and optical data for test case 1 (1-h nozzle, 100 bar injection pressure). As mentioned earlier, a 4°CA ramp is used to model the transient duration, showing a good agreement with schlieren images. With the nominal SOI = -140°CA, the first traces of the jet are visible in the cylinder at -137°CA, which agrees with the assumption of actual SOI = -137°CA. The jet penetration in the numerical results seems to match the optical data, even though the actual jet direction is not well captured, as seen in Figure 8 at -135°CA. Apart from tolerances in nozzle fabrication, the jet might also deviate slightly due to the flow inside of the injector, which is not part of the current calculation. As a consequence, in the CFD results the jet impinges the wall higher compared to PLIF data, with consequent difference in terms of jet location at -130°CA.

Furthermore, the assumption of the transient duration can also have an effect. Compared to previous numerical results [17,18], in this paper the transient is longer, leading to a “slower” jet penetration (see comparison at -130°CA), which nevertheless agrees with schlieren data. This is a first indication that a linear transient and a trapezoidal injection profile cannot be the proper input to achieve perfect agreement between numerical and experimental results.

The evolution of the hydrogen jet is well captured by numerical simulation throughout the compression stroke, even after the multiple impingements on the cylinder walls. Two main issues can be highlighted in Figure 8. First, the CFD results can qualitatively capture the stratification within the jet (the region with highest values of fuel mole-fraction is located below the exhaust valve at -70°CA, below the injector at -55°CA and below the intake valve at -30°CA), nevertheless the fuel dispersion is under-predicted, leading to a (quantitative) disagreement in fuel concentration. Overall, the gradient of fuel concentration in the optical data is much smoother than in the CFD results. All the versions of the k-ε model (standard, RNG, Realizable) have been previously tested [18] and have provided similar results. Also, tuning of the k-ε Realizable model has been performed, showing better (quantitative) results in terms of concentration values but simultaneous loss of qualitative information on mixture stratification [18]. One of the main hypotheses that the authors have developed is that the RANS approach simply cannot accurately predict the local fuel diffusion since the smallest scales of turbulence are modeled instead of being directly calculated. This conclusion suggests the use of a more detailed approach (LES) in the future, in order to increase the level of detail and the accuracy of the numerical simulations.

Also, the grid resolution at the cylinder walls might play a role in the disagreement between experiments and modeling. In this study, the overall grid resolution is decreased compared to a previous study [18], while increased near the nozzle, to achieve higher accuracy within the supersonic jet while avoiding prohibitive computational times. As a consequence, the jet behavior at the cylinder walls might be not well predicted by numerical simulations, and this might influence the fuel distribution in the direction orthogonal to the wall. Wall refinement and the use of a more sophisticated wall treatment approach are currently under investigation.

It is worth noting that in this study the range of hydrogen mole fraction is dynamically varied during the compression stroke in order to highlight the differences between numerical and optical data. Still, after more than 100°CA, the computational code is able to provide accurate results in terms of fuel stratification, even though the mixture tends to progressively become homogeneous when the piston approaches TDC.

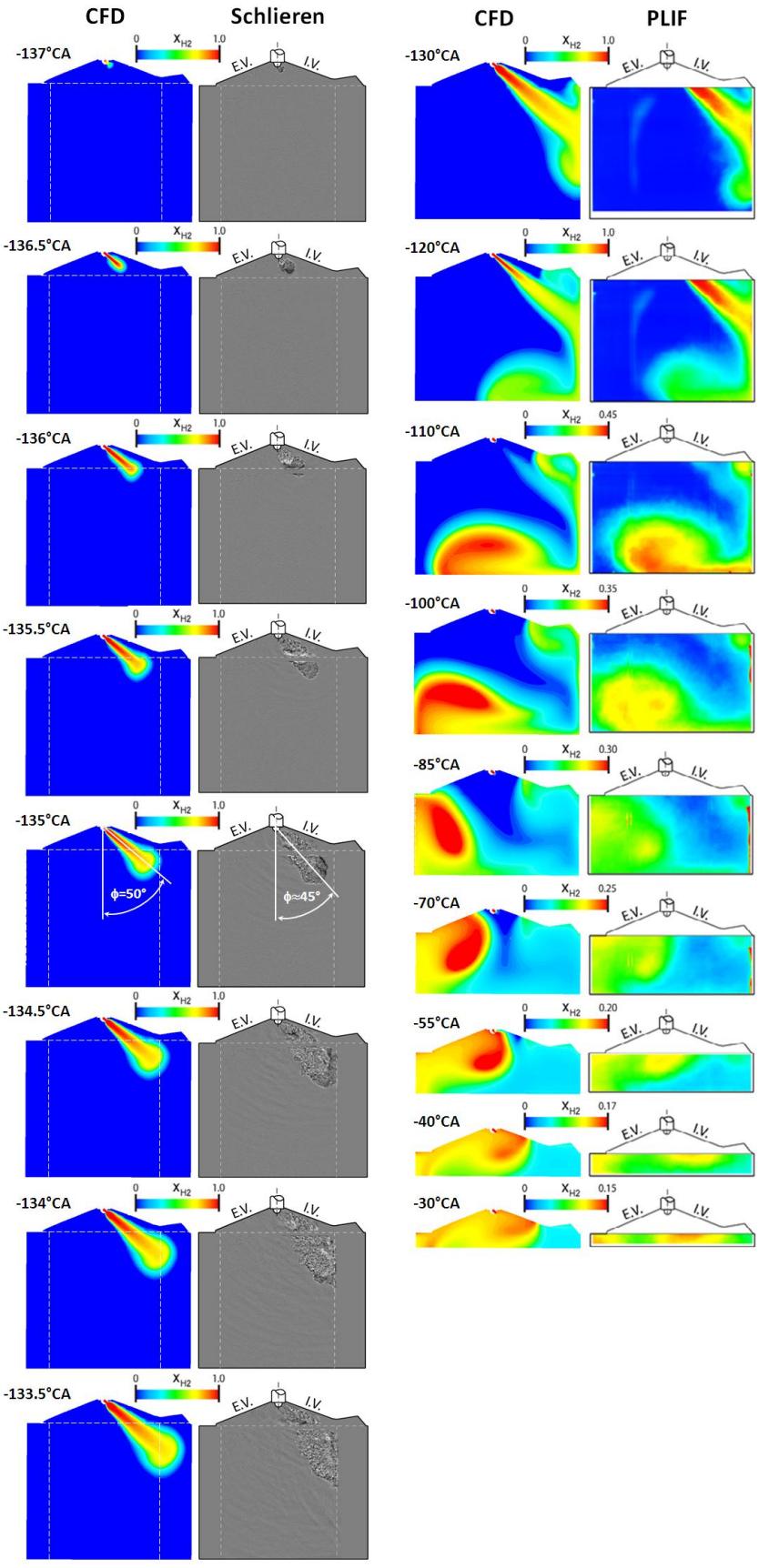

Figure 8 Comparison between CFD and optical (Schlieren and PLIF) data for test case 1 (1-h, 100 bar)

TEST CASE 2 (1-H 25BAR)

Figure 9 compares numerical and optical data for test case 2 (1-h nozzle, 25 bar injection pressure). The comparison with schlieren data does not show differences between modeling and experiments in terms of jet direction, unlike what is observed for test case 1 (1-h nozzle, 100 bar injection pressure). This suggests that the nozzle internal flow might influence the jet direction as a direct effect of the injection pressure. Also, jet penetrates faster in CFD results than in optical data during early injection (see Figure 9 at -133°CA), while in the PLIF data the hydrogen jet impinges the cylinder walls earlier than in the numerical results (-129°CA). These results may again indicate that the linear-transient model is somewhat lacking and may need refinement, depending on the importance of early jet behavior in the objectives of simulation. It is also possible that these minor differences are due to limited repeatability of the injection process, since PLIF and schlieren images were taken several months apart.

Overall, the agreement during the entire compression stroke is remarkable, suggesting that the lower jet velocity might play a role in ensuring more accurate results than the 1-h 100 bar case when using the same computational grid. Results up to -70°CA do not allow emphasizing the difference in terms of fuel concentration between optical and CFD data, due to the wide range of values represented (injection is still taking place, since EOI = -59.5°CA for test case 2). However, at -50°CA and -30°CA, where the maximum H_2 mole fraction values are reduced to 0.45 and to 0.2, a remarkable agreement can be observed between experiments and modeling.

TEST CASE 3 (13-H 86BAR)

Figure 10 shows the comparison between numerical and optical data for test case 3 (13-h nozzle, 86 bar injection pressure). This condition represents an extreme case, in that the jet-to-jet interaction leads to complete merging of all jets into a single jet at the nozzle exit. The phenomenon, known as Coanda effect, stems from the lack of air entrainment in the jet due to the presence of another jet in close proximity. Figure 7d has shown how the jets merging takes place downstream of each Mach disk, where each jet deviates towards its closest neighbor jet and due to the nozzle symmetry all the side jets are pulled towards the central jet. At the end of Mach disk, the jet becomes subsonic, and that is the moment (see Figure 7c) where each jet suffers from the Coanda effect, since air entrainment is limited by the presence of a close jet. In this zone the requirements for the grid resolution are more stringent and particular care has to be taken when generating the computational mesh, even relatively far from the Mach disk.

The comparison between CFD and schlieren data shows that the assumption of 3°CA delay in SOI is not exactly correct for this case. Not clearly visible in Figure 10 at -137°CA, the hydrogen jet is already coming out from the nozzle, but the numerical simulation predicts a higher penetration at the beginning of the injection process (see Figure 10 at -136°CA). Once again, the assumed injection profile might be the reason for this disagreement. It is worth pointing out that the turbulence on very small scales might have a role too. High turbulence at the jet boundaries, clearly visible in the schlieren data and roughly modeled in numerical simualtion, might increase the jet-to-jet interaction and slow each jet down. Therefore, the RANS approach in this operating condition might suffer from higher inaccuracy than for the single-hole nozzle cases.

During the merging, the resulting jet propagates slower in the numerical results compared to optical data. The jet shape in CFD data also does not exactly match the schlieren images. Higher accuracy might be gained by extending the high resolution domain further in the computational mesh, at least to the pentroof – cylinder interface. Still, at -130°CA the penetration in CFD data is slightly higher than in PLIF data. For this nozzle it is difficult to evaluate the assumption of injection transient, since the jet-to-jet interaction and the quality of the mesh do not make the comparison between experiments and modeling as clear as in the single-hole cases.

The agreement is remarkable at -120°CA and -110°CA. Later in the compression, the location of the hydrogen clouds is still well predicted. The rich zones remain located close to the piston during the entire compression stroke. Nevertheless, here the under-prediction of fuel dispersion is even more pronounced than in the previous two cases. The mixture stratification at the end of compression (-30°CA) is not sufficiently well predicted and the lack of optical information in the pent-roof does not improve the quality of the comparison. Two main rich zones can be observed at -40°CA, the richer one being located in the intake quenching zone. Numerical results show a similar behavior, however the fuel dispersion is significantly different and this greatly affects the numerical prediction in terms of final mixture stratification.

The multi-hole nozzle is the worst case scenario to be simulated, especially when a high number of holes are considered. The complex physical phenomena involved in the under-expanded region together with the jet-to-jet interaction might lead to the inaccurate prediction of the air entrainment in the proximity of the nozzle exit, which might increase the disagreement between numerical and experimental results in terms of fuel dispersion, since the mixing is faster in this case. Nevertheless, even in this case there is a good consistency between CFD and optical data in terms of jet penetration and evolution. Future investigations will focus on jet behavior at cylinder walls (wall boundary layers and more sophisticated wall functions) and higher-detail simulations (higher grid resolution, LES) in order to further improve the numerical predictions for all the cases shown in this paper.

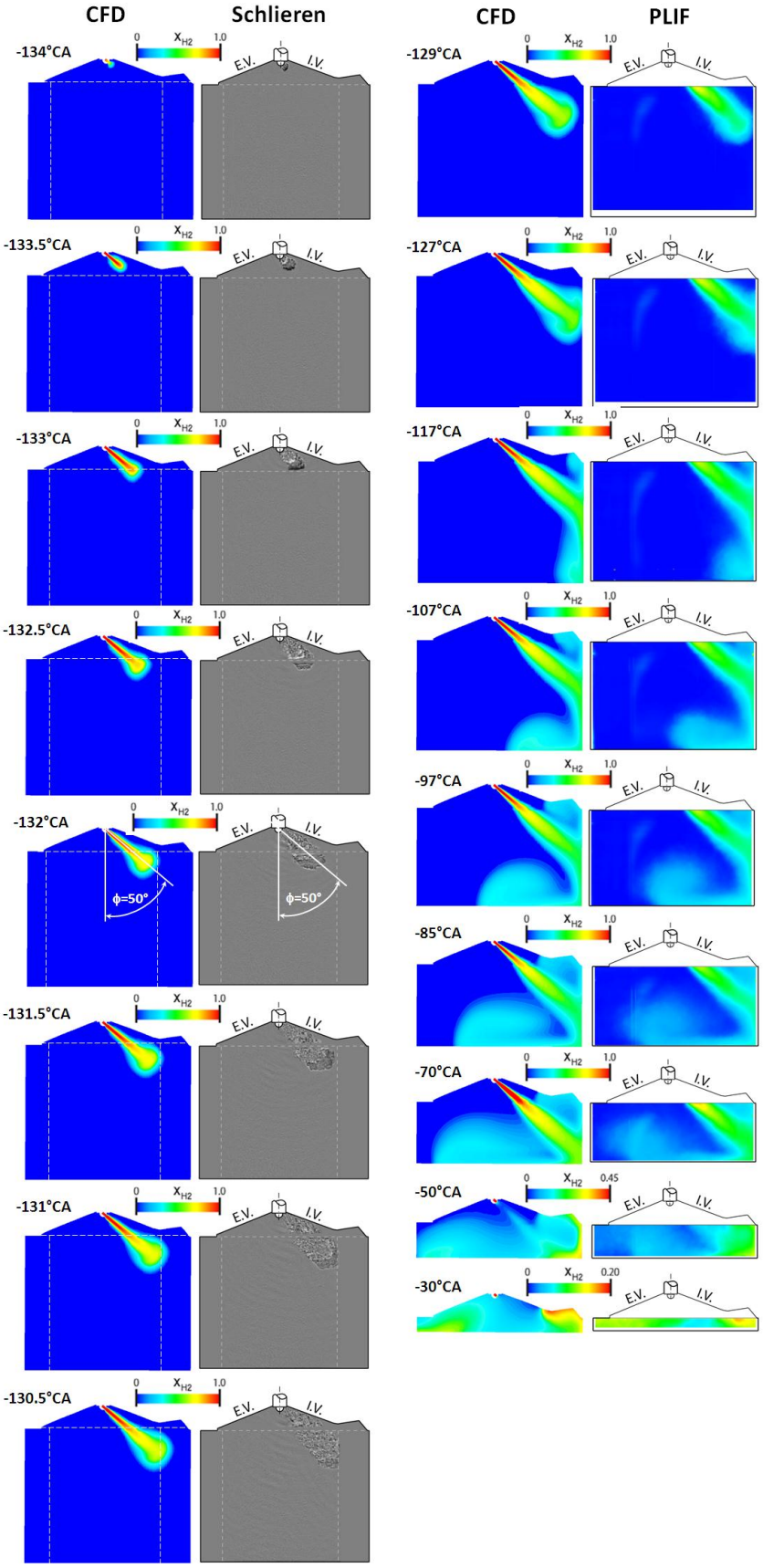

Figure 9 Comparison between CFD and optical (Schlieren and PLIF) data for test case 2 (1-h, 25 bar)

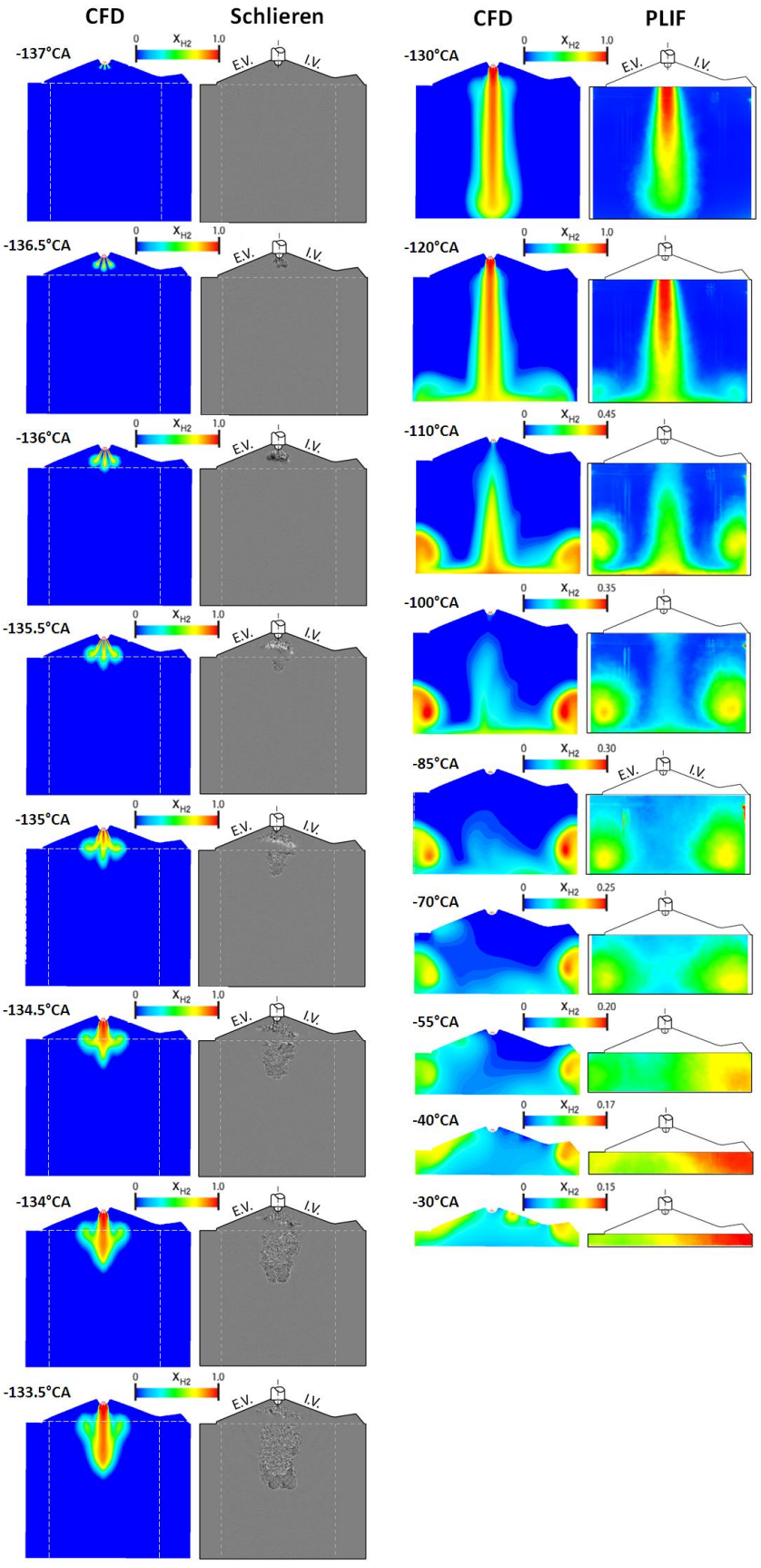

Figure 10 Comparison between CFD and optical (Schlieren and PLIF) data for test case 3 (13-h, 86 bar)

CONCLUSIONS

A major challenge for a direct injection engine is the optimization of the mixture formation process. Properly validated numerical simulation can become a powerful tool for the optimization of DI H_2-ICEs, however its accuracy can be validated only by the comparison with experimental data on jet penetration and mixture stratification from an optically accessible engine.

This paper extends the initial validation of numerical results by a CFD-RANS approach to a wider range of cases, including high and low injection pressure and single- and multi-hole nozzles. Optimized computational grids and the k-ε Realizable turbulence model are used and injection profile assumptions are discussed, providing a comprehensive analysis of the main numerical features that need to be taken into account in the simulation of a gaseous fuel DI engine.

The comparison with optical data shows a remarkable agreement in terms of jet penetration and overall evolution for all the examined cases. The agreement remains good along the entire compression, even after multiple impingements with the cylinder walls. Fuel dispersion is under-predicted in all the examined cases, with the highest disagreement for high injection pressure.

The multi-hole nozzle shows the least accurate results in terms of both initial jet penetration and final fuel distribution. The hypothesis is that the jet-to-jet interaction occurring in the under-expanded region is not captured with the current level of detail.

Increasing grid resolution along the jet direction, using more accurate wall treatment, and performing higher detail simulations (LES) to describe turbulence are identified by the authors as the possible key for an improvement of the quality of numerical predictions. However, in the current state, CFD already shows remarkable results, making it a useful tool to optimize injection parameters and nozzle configuration in order to increase efficiency and reduce the emissions in a hydrogen-fuelled DI engine.

ACKNOWLEDGMENTS

This manuscript has been created by U-Chicago Argonne, LLC, Operator of Argonne National Laboratory ("Argonne") and Sandia National Laboratories ("Sandia"). Argonne, a U.S. Department of Energy Office of Science laboratory, is operated under Contract No. DE-AC02-06CH11357. Sandia is a multi-program laboratory operated by Sandia Corporation, a Lockheed Martin Company, for the United States Department of Energy's National Nuclear Security Administration under contract DE-AC04-94AL85000. The U.S. Government retains for itself, and others acting on its behalf, a paid-up nonexclusive, irrevocable worldwide license in said article to reproduce, prepare derivative works, distribute copies to the public, and perform publicly and display publicly, by or on behalf of the Government.

The authors would like to thank especially Brad Boyer and Matt Younkins from Ford Motor Company for their invaluable support of the DI-H2ICE project. This research is funded by DOE's Vehicle Technologies Program, Office of Energy Efficiency and Renewable Energy, with Gurpreet Singh as the program manager.

REFERENCES

1. S. Verhelst, R. Sierens, A Critical Review of Experimental Research on Hydrogen Fueled SI Engines, SAE Technical Paper 2006-01-0430, 2006.
2. S. Verhelst, T. Wallner, Hydrogen-fueled internal combustion engines, Progress in Energy and Combustion Science, Volume 35, Issue 6, December 2009, Pages 490-527, 2009.
3. C. M. White, R. R. Steeper, A. E. Lutz, The hydrogen-fueled internal combustion engine: a technical review. Int. J. Hydrogen Energy 31:1292-1305, 2006.
4. H. Obermair, R. Scarcelli, T. Wallner "Efficiency Improved Combustion System for Hydrogen Direct Injection Operation", SAE Technical Paper 2010-01-2170, 2010.
5. S. Tanno, Y. Ito, R. Michikawauchi, M. Nakamura, H. Tomita, "High-Efficiency and Low-NOx Hydrogen Combustion by High Pressure Direct Injection", SAE Technical Paper 2010-01-2173, 2010.
6. U.S. Department of Energy, FreedomCAR and Fuel Technical Partnership Technical Goals, Washington, D.C, 2002.
7. A. Wimmer, T. Wallner, J. Ringler, F. Gerbig,, H2-Direct Injection — A Highly Promising Combustion Concept, SAE Technical Paper 2005-01-0108, 2005.
8. T. Wallner, A. M. Nande, J. Naber, Evaluation of Injector Location and Nozzle Design in a Direct-Injection Hydrogen Research Engine, SAE Technical Paper 2008-01-1785, 2008.
9. T. Wallner, A. M. Nande, J. Naber, Study of Basic Injection Configurations using a Direct-Injection Hydrogen Research Engine, SAE Technical Paper 2009-01-1418, 2009.

10. T. Wallner, R. Scarcelli, A. M. Nande, J. Naber, Assessment of Multiple Injection Strategies in a Direct Injection Hydrogen Research Engine, SAE Technical Paper 2009-01-1920, 2009.
11. T. Wallner, N. Matthias, R. Scarcelli, Influence of injection strategy in a high-efficiency hydrogen direct injection engine, submitted for publication at JSAE / SAE 2011 Powertrains Fuels & Lubricants Meeting, paper proposal JSAE 20119044, 2011.
12. A. M. Nande, T. Wallner, Influence of Water Injection on Performance and Emissions of a Direct-Injection Hydrogen Research Engine, SAE Technical Paper 2008-01-2377, 2008.
13. T. Wallner, A. Nande, R. Scarcelli, Evaluation of exhaust gas recirculation (EGR) in combination with direct injection (DI) on a Hydrogen Research Engine, presented at World Hydrogen Technology Convention, New Delhi/India, 2009.
14. V. M. Salazar, S. A. Kaiser, An Optical Study of Mixture Preparation in a Hydrogen-fueled Engine with Direct Injection Using Different Nozzle Designs, SAE Technical Paper 2009-01-2682, 2009.
15. S. A. Kaiser, C. M. White, PIV and PLIF to Evaluate Mixture Formation in a Direct-Injection Hydrogen-Fueled Engine, SAE Technical Paper 2008-01-1034, 2008.
16. V. M. Salazar, S. A. Kaiser, Influence of the In-Cylinder Flow Field (Tumble) on the Fuel Distribution in a DI Hydrogen Engine Using a Single-Hole Injector, SAE Technical Paper 2010-01-0579, 2010.
17. R. Scarcelli, T. Wallner, H. Obermair, V.M. Salazar, S.A. Kaiser, "CFD and Optical Investigations of Fluid Dynamics and Mixture Formation in a DI-H2 ICE", ASME ICEF Conference 2010 (San Antonio, Texas, USA), ASME Paper ICEF2010-35084, 2010.
18. R. Scarcelli, T. Wallner, N. Matthias V.M. Salazar, S.A. Kaiser, Numerical and Optical Evolution of Gaseous Jets in Direct Injection Hydrogen Engines, SAE Technical Paper 2011-01-0675, 2011.
19. V. M. Salazar, S. A. Kaiser, F. Halter, Optimizing Precision and Accuracy of Quantitative PLIF of Acetone as a Tracer for Hydrogen Fuel, SAE Technical Paper 2009-01-1534, 2009.
20. M. C. Thurber, F. Grisch, B. J. Kirby, M. Votsmeier, R. K. Hanson, Measurements and Modeling of Acetone Laser-Induced Fluorescence with Implications for Temperature-Imaging Diagnostics, Appl. Optics 37 (1998) 4963-4978, 1998.
21. M. C. Thurber, R. K. Hanson, Pressure and composition dependences of acetone laser-induced fluorescence with excitation at 248, 266, and 308 nm , Appl. Phys. B - Lasers Opt. 69 (1999) 229-240.
22. C. Espey, J. E. Dec, T. A. Litzinger, D. A. Santavicca, Planar laser rayleigh scattering for quantitative vapor-fuel imaging in a diesel jet, Combust. Flame 109 (1997) 65-86, 1997.
23. W. Hwang, J. E. Dec, M. Sjoberg, Fuel Stratification for Low-Load HCCI Combustion: Performance & Fuel-PLIF Measurements, SAE Technical Paper 2007-01-4130, 2007.
24. C.-N. Yeh, T. Kamimoto, H. Kosaka, S. Kobori, Quantitative Measurement of 2-D Fuel Vapor Concentration in a Transient Spray Via a Laser-Induced Fluorescence Technique, SAE Technical Paper 941953, 1994.
25. G.S.Settles, *"Schlieren and Shadowgraph Techniques"*, Springer, Berlin, 2001.
26. L.M. Pickett, S. Kook, and T.C. Williams, "Visualization of Diesel Spray Penetration, Cool-Flame, Ignition, High-Temperature Combustion, and Soot Formation Using High-Speed Imaging," *SAE Technical Paper* 2009-01-0658, 2009.
27. J. Abraham, "What is Adequate Resolution in the Numerical Computations of Transient Jets?", SAE Technical Paper 970051, 1997.

NOMENCLATURE

BTE	Brake Thermal Efficiency
°CA	Degree Crank Angle
CCD	Charge-Coupled Device
CFD	Computational Fluid Dynamics
CMOS	Complementary Metal Oxide Semiconductor
COV	Coefficient of Variation
DI	Direct Injection
DNS	Direct Numerical Simulation
EGR	Exhaust Gas Recirculation

EOI	End of injection
H_2	Hydrogen
ICE	Internal Combustion Engine
IMEP	Indicated Mean Effective Pressure
IVC	Intake Valve Closing
LED	Light Emitting Diode
LES	Large Eddy Simulation
N_2	Nitrogen
Nd:YAG	Neodymium-doped Yttrium Aluminum Garnet
NO_X	Nitrogen Oxides
PFI	Port Fuel Injection
PIV	Particle Image Velocimetry
PLIF	Planar Laser-Induced Fluorescence
RANS	Reynolds-Averaged Navier-Stokes
RNG	Renormalization Group
RPM	Revolution per Minute
SI	Spark-Ignition
SOI	Start of Injection
TDC	Top Dead Center
1-h	Single-Hole Nozzle
13-h	13-Hole Nozzle
Ma	Mach Number
λ	Air/Fuel Ratio

CONTACT INFORMATION

Riccardo Scarcelli, Ph.D.
Argonne National Laboratory • Energy Systems Division
Building 362 • 9700 South Cass Avenue • Argonne, IL 60439-4815 • www.anl.gov
Phone: 630.252.6940 • Fax: 630.252.3443 • Email: rscarcelli@anl.gov